Experimental Study of Fast-Transient Flow Boiling Phenomena in a Tube

Yong-Seok Choi *, Dong-Hoon Kam, Jong-Kuk Park, Sang-Ki Moon
Innovative System Safety Research Division, Korea Atomic Energy Research Institute, 111 Daedeok-daero 989 Beon-gil, Yuseong-gu, Daejeon, 34057
Corresponding author: cys@kaeri.re.kr

1. Introduction

The accidental insertion of reactivity to the reactor core can cause a sudden increase in the fission rate and reactor power, leading to a reactivity-initiated accident (RIA). Most studies on the RIA safety focused on pre-DNB (i.e., departure from nucleate boiling) failure mechanisms such as the pellet-clad mechanical interaction (PCMI) rather than the post-DNB phenomena. This led to a lack of knowledge related to the thermal hydraulic phenomena during the RIA [1-3].

We constructed a thermal hydraulic test facility for RIA safety research to study the effect of various flow conditions on fast-transient flow boiling phenomena. In this paper, recent experimental results showing different transient boiling heat transfer characteristics are presented according to wide range of pressure and heating rate.

2. Methodology

2.1 Experimental Apparatus

Figure 1 shows the schematics of the test facility which was designed to reproduce the thermal-hydraulic conditions during the RIA of PWR. The operating ranges of the facility are as followings:

- Pressure: 0.5~16.0 MPa
- Test section flow rate: 0~0.3 kg/s
- Maximum water temperature: 340 ℃
- Pulse power: up to 450 kW
- Pulse width: 20 ms ~ 1.25 sec

The test section is a vertically placed Inconel-600 tube with upward flow. Inner diameter and wall thickness of the tube are 8 mm and 1 mm, respectively. Direct Joule heating is applied on the tube with a step pulse power. Heating length is 500 mm, and corresponding volumetric power is up to 21.8 GW/m^3 which results tube heating rate of about 4,100 K/s.

A high-speed infrared pyrometer (IGA 6/23 advanced, LUMASENSE Tech.) is adopted to measure surface temperature of the tube. The pyrometer has a measurable temperature range of 75 to 1,300 ℃ and an applicable wavelength spectrum of 2 to 2.6 μm. Its minimum response time, t90, is 0.5 milliseconds. A matte black body paint (Rust-Oleum, Specialty High Heat) is sprayed on the tube surface to get a stable emissivity value of 0.95. Temperature measured by the pyrometer is checked using thermocouples attached on the tube surface. While varying the tube temperature slowly, the temperature difference between the pyrometer and the thermocouple is confirmed to be within ±3℃ in the whole experimented ranges.

A high-speed data acquisition system (PXIe series, National Instruments) is adopted to collect the experimental data. Voltage and current applied on the tube and its surface temperature are sampled simultaneously with a 5 kHz frequency. To get the voltage, an electric wire is attached on each bus-bar to draw a potential voltage. The current signal is obtained from two parallel shunts which have 3,000 amperes capacity (Manufacturer: Yokogawa) for each. Temporal power is deduced by multiplying the voltage and current. Flow rate, pressures, and water temperatures are collected in 0.1 kHz frequency. Flow rate is obtained from the mass flow meter (RHM 08, Rheonik) having a rated uncertainty less than 0.1%. Pressures are detected from an in-line type gauge pressure transmitter (Manufacturer: Rosemount) that has 0.025% span accuracy. Inlet and outlet water temperatures are measured by a K-type thermocouple (Manufacturer: Omega) that has 1.5℃ tolerance in the experimented temperature ranges.
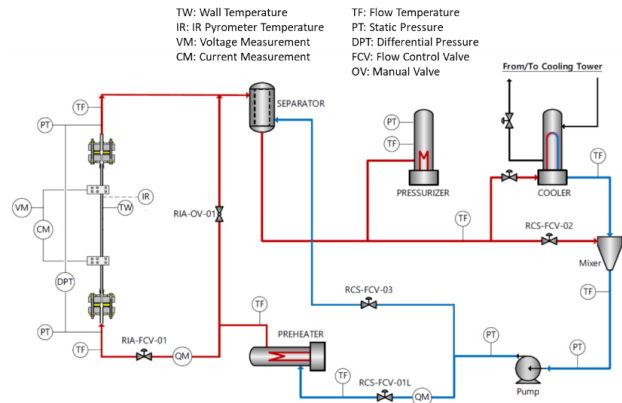
Fig. 1. Schematic of the test facility.

2.2 Inverse Heat Conduction Calculation

In this study, temperature and heat flux on the boiling surface are unknown. This is an ill-posed heat conduction problem that cannot be solved by a direct heat conduction equation since no boundary conditions exist on the inner surface of the tube. To solve the problem, the spatial marching Inverse Heat Conduction (IHC) calculation scheme [4, 5] is adopted. In this

scheme, if temperature data at the spatial node m=0 is given for sufficient time steps, the temperature values at the next spatial node can be obtained sequentially. After the numerical solution is obtained for all time steps at a given spatial node, then the calculation node is proceeded to the next spatial node. By repeating this process until the final node is reached, all the temperature information can be solved. This is in contrast to the method for solving direct problems where the solution is obtained for all spatial nodes at a given time step before proceeding to the next time step. Finally, the heat flux at the inner surface is calculated using energy balance in control volume of the final node.

The ill-posed nature of the IHC problem amplifies instability from the blended noise in the calculation inputs. Therefore, an effective noise reduction scheme is essential to retrieve a reliable solution from the measured data. A frequency filtering method is adopted to remove random noises from the surface temperature and injected power records. A low-pass Gaussian filter whose impulse response is a Gaussian function is used as the frequency filter. The filtering process essentially consists of three steps: (1) Fourier transform of the sampled data, (2) multiplication of the transformed data and the filter in a frequency domain, and (3) inverse Fourier transform of the filtered data. This numerical filtering process greatly enhances the IHC calculation results.

3. Results

3.1 Effect of Pressure

Effect of system pressure is investigated on the fast-transient flow boiling phenomena with varying tube inlet pressure from 1 MPa to 15 MPa. Mass flux and subcooing conditions are fixed to 3500 kg/m^{2}s and 300 kJ/kg, respectively. Step pulse power of 17.0 GW/m^3 is applied with adjusting pulse width to produce DNB to film boiling transition during the pulse injection.

(a) 1 MPa   (b) 15 MPa
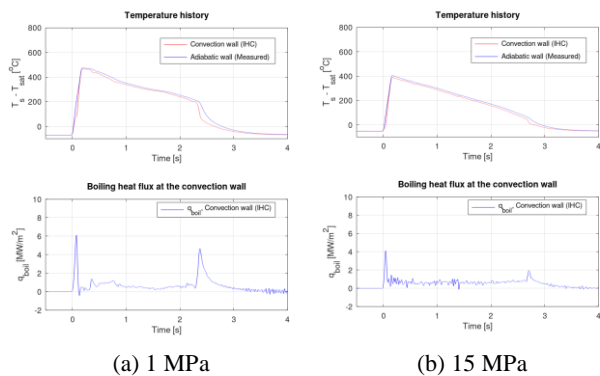
Fig. 2. Variation of wall temperatures and heat flux on the boiling surface.

(a) 1 MPa   (b) 15 MPa
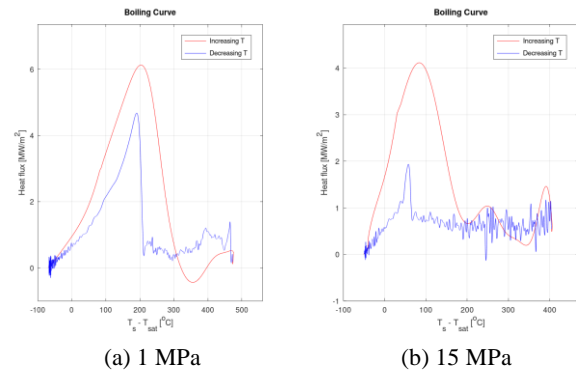
Fig. 3. Fast-transient boiling curve.

Fig. 2 shows the wall temperatures and the heat flux histories after the pulse injection. Adiabatic wall temperature which is measured by the pyrometer and the convection wall temperature which is obtained by the IHC calculation are plotted together. The pulse starts at time t = 0 and the wall temperatures also start to rise rapidly. During the temperature rise, DNB and film boiling transition occur sequentially as the heat flux peak and subsequent drop indicates. After the pulse ends, the temperatures start to drop gradually by the continued film boiling heat transfer until the minimum stable film boiling temperature is reached. The sudden drop of the temperature and the second heat flux spike are due to the rewetting of the tube wall. Fig. 3 represents the boiling curve during the fast-transient flow boiling. The red-line indicates the boiling curve during the heating phase while the blue-line indicates the curve during the cooling phase. From the boiling curve, the heat flux variation as a function of the wall temperature and important characteristic temperatures, such as critical (DNB) temperature, minimum stable film boiling temperature, rewetting temperature, can be deduced.

The critical heat flux at the DNB (q''_{crit}) and the heat flux peak during the rewetting (q''_{wet}) are plotted according to the pressure in Fig. 4. Steady-state CHF obtained from the look-up table is also plotted in the figure.
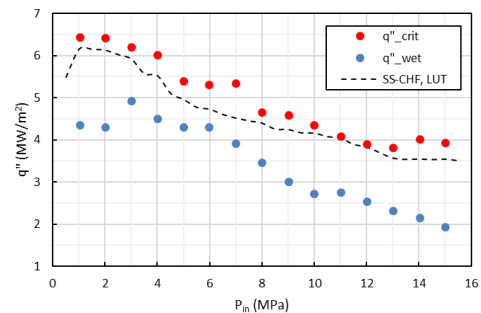
Fig. 4. Effect of pressure on the peak heat fluxes.

The q''_{crit} are about 1% to 18% higher than the steady-state CHF values. The increment is not consistent to the

pressure. Maximum increment occurs at 7 MPa and minimum increment occurs at 11 MPa. Contrarily, the q''_{wet} are about 9% to 45% lower than the steady-state CHFs. Minimum decrement occurs at 6 MPa and maximum decrement occurs at 15 MPa.
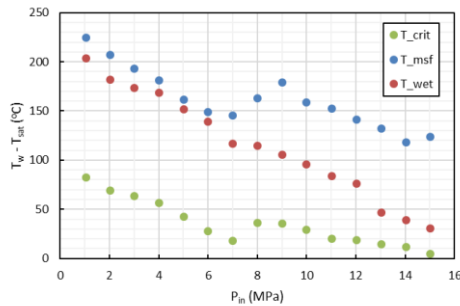
Fig. 5. Effect of pressure on critical temperature, minimum stable film temperature, and rewetting temperature.

Fig. 5 shows the critical temperature (T_{crit}), minimum stable film temperature (T_{msf}), and rewetting temperature (T_{wet}) according to the pressure. The temperatures show generally decreasing trends as the pressure increases. However, the T_{crit} and T_{msf} also show increasing trends for 7 MPa to 9 MPa ranges. These complex behaviors of the characteristic temperatures seem to be related with the nucleation and bubble development mechanisms [6].

3.2 Effect of Heating Rate

Effect of wall heating rate is investigated with varying the pulse power from 4.8 GW/m^3 to 21.8 GW/m^3. Fig. 6 shows q''_{crit} distribution according to the pulse power. q''_{wet} is not relevant to the pulse power since the rewetting occurs during the cooling phase. q''_{crit} plots show increasing trends regardless to the pressure condition up to about 14 GW/m^3. When the pulse power is further increased, the q''_{crit} seems to be saturated as the plots for 5 MPa and 10 MPa show. In 15 MPa case, large fluctuations are observed in the present data.

Fig. 7 show T_{crit} and T_{msf} distributions according to the pulse power. T_{wet} is not relevant to the pulse power since it occurs during the cooling phase. T_{crit} does not show any relation to the heating rate while the T_{msf} is strongly affected. However, the effect of pressure is not so significant for T_{msf} compare to the heating rate.

4. Conclusions

Effects of system pressure and heating rate are investigated on fast-transient flow boiling phenomena. Established experimental facility and experimental methods including the inverse heat conduction calculation show good applicability on studying the phenomena. As results, variations of critical heat flux, rewetting heat flux, critical temperature, minimum

stable film temperature, and rewetting temperature are determined. These values will be used to obtain fast-transient flow boiling curve to model the heat flux under abrupt power excursion situation. Currently we are gathering more experimental data to get concrete statistical information. In addition, the effect of mass flux and inlet subcooling will be also obtained using the same facility and methods.
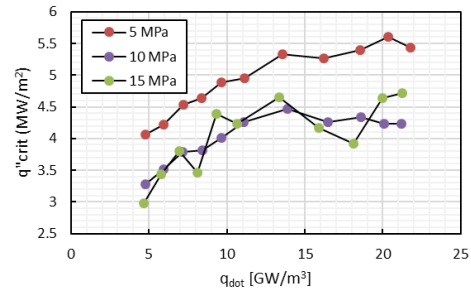
Fig. 6. Effect of heating rate on critical heat flux.

(a) T_{crit} (b) T_{msf}
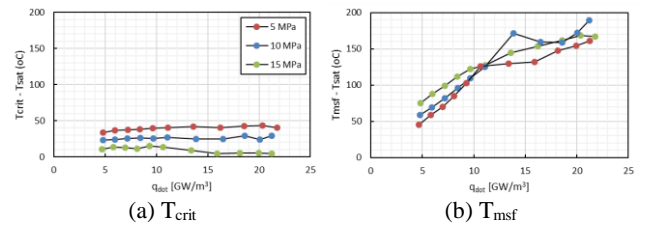
Fig. 7. Effect of heating rate on critical temperature and minimum stable film temperature.

REFERENCES

[1] V. Bessirion, "Modeling of clad-to-coolant heat transfer for RIA applications," J. Nucl. Sci. Technol., 44(2), pp. 211-221 (2007).
[2] R. Visentini, C. Colin, and P. Ruyer, "Experimental investigation of heat transfer in transient boiling," Exp. Therm. Fluid Sci., 55, pp 95-105 (2014).
[3] X. Zhao, A. Wysocki, R. Salko, et al., "Mechanistic modeling of departure from nucleate boiling under transient scenarios," in Proc. Int. Cong. on Advances in Nucl. Power Plants, Charlotte, North Carolina, Apr 8-11, 2018 (2018).
[4] C. F. Weber, "Analysis and solution of the ill-posed inverse heat conduction problem," Int. J. Heat Mass Transf. 24(11), pp. 1783-1792 (1981).
[5] M. Morse and R. Feshbach, Methods of theoretical physics, McGraw-Hill (1953).
[6] T. Hibiki and M. Ishii, "Active nucleation site density in boiling systems," Int. J. Heat Mass Transf. 46, pp. 2587-2601 (2003).